A minimal mathematical model combining several regulatory cycles from the budding yeast cell cycle

K. Sriram, G. Bernot and F. Képès

Abstract: A novel topology of regulatory networks abstracted from the budding yeast cell cycle is studied by constructing a simple nonlinear model. A ternary positive feedback loop with only positive regulations is constructed with elements that activates the subsequent element in a clockwise fashion. A ternary negative feedback loop with only negative regulations is constructed with the elements that inhibit the subsequent element in an anticlockwise fashion. Positive feedback loop exhibits bistability, whereas the negative feedback loop exhibits limit cycle oscillations. The novelty of the topology is that the corresponding elements in these two homogeneous feedback loops are linked by the binary positive feedback loops with only positive regulations. This results in the emergence of mixed feedback loops in the network that displays complex behaviour like the coexistence of multiple steady states, relaxation oscillations and chaos. Importantly, the arrangement of the feedback loops brings in the notion of checkpoint in the model. The model also exhibits domino-like behaviour, where the limit cycle oscillations take place in a stepwise fashion. As the aforementioned topology is abstracted from the budding yeast cell cycle, the events that govern the cell cycle are considered for the present study. In budding yeast, the sequential activation of the transcription factors, cyclins and their inhibitors form mixed feedback loops. The transcription factors that involve in the positive regulation in a clockwise orientation generates ternary positive feedback loop, while the cyclins and their inhibitors that involve in the negative regulation in an anticlockwise orientation generates ternary negative feedback loop. The mutual regulation between the corresponding elements in the transcription factors and the cyclins and their inhibitors generates binary positive feedback loops. The bifurcation diagram constructed for the whole system can be related to the different events of the cell cycle in terms of dynamical system theory. The checkpoint mechanism that plays an important role in different phases of the cell cycle are accounted for by silencing appropriate feedback loops in the model.

1 Introduction

Cyclical organisations of biological networks are widely seen in neurobiology [1], immunology [2] and in the chemical systems [3]. Theoretical and experimental models such as 'circulator' [4] and 'repressilator' [5], respectively, are constructed to get insight into the organization and functioning of the cyclical biological networks. Another interesting case of a cyclical network is the Hypercycle – a closed reaction network which connects autocatalytic or self-replicative units through a cyclic linkage that form a closed feedback loop [6]. Among the three examples cited, circulator model has both positive and negative feedback loops, whereas repressilator and hypercycles have only negative and positive feedback loops, respectively. In naturally occurring biological systems, both positive and negative feedback loops play a vital role that together contributes to the precise functioning and robustness of a system [7].

Before embarking further, the terms that are used in this article for describing the regulatory networks are defined. The term feedback loop here is used to denote whenever the element influences its own production or inhibition directly or through a path of interactions with several dynamical elements. Positive and negative feedback loops are distinguished by the parity of negative interactions among the dynamical elements. If the number of negative interactions are even (odd), the feedback loop is positive (negative). For example, in Fig. 1*e*, 'Y1' negatively regulates 'Y2', which in turn negatively regulates 'Y1' completing the positive feedback loop. Both types of feedback loops are observed widely in many regulatory networks like cell cycle [8, 9] and circadian rhythms [10]. Negative feedback loops provide homeostasis or oscillations, positive feedback loops cause multistationarity that may be essential for epigenetic modifications and inheritance [11]. Positive feedback loops also cause instability, but are important to prolong and amplify the response of a weak signal. Various configurations of feedback loops have been studied and some of the common configurations that have been dealt and analysed extensively are given in Fig. 1.

In Fig. 1 are shown the one and two element regulatory positive and negative feedback loops that are the common building blocks of many interesting complex regulatory networks. Analysis of these building blocks or the combination thereof provides insight into the working and functioning of the biological systems [5, 12–16]. The feedback loops

doi:10.1049/iet-syb:20070018

Paper first received 3rd April and in revised form 13th June 2007

The authors are with the Epigenomics Project, 523, Place des Terrasses de l' Agora, Tour Evry 2, Genopole®, Evry, 91000 France

F. Kepès is also with ATelier de Genomique Cognitive, CNRS UMR8071/ Genopole®

E-mail: sridelin@yahoo.co.in

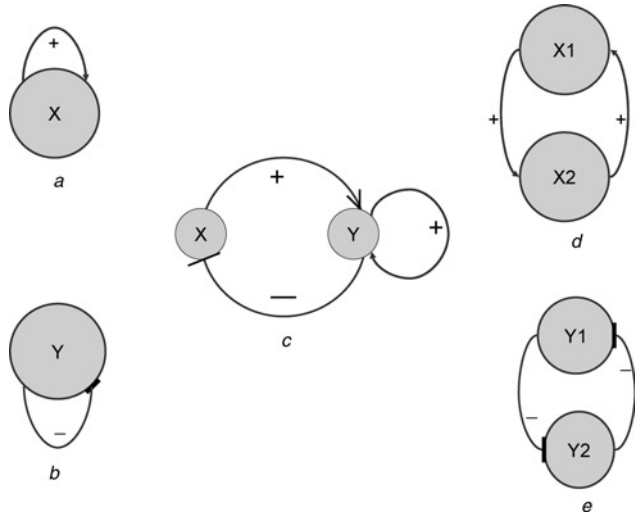

Fig. 1 *Common feedback loops studied in the biological systems*

a and *b* One element positive and negative feedback loops
c Two element mixed feedback loop
d and *e* Two element positive and negative feedback loops. Feedback loops are identified according to the parity of negative interactions among the elements

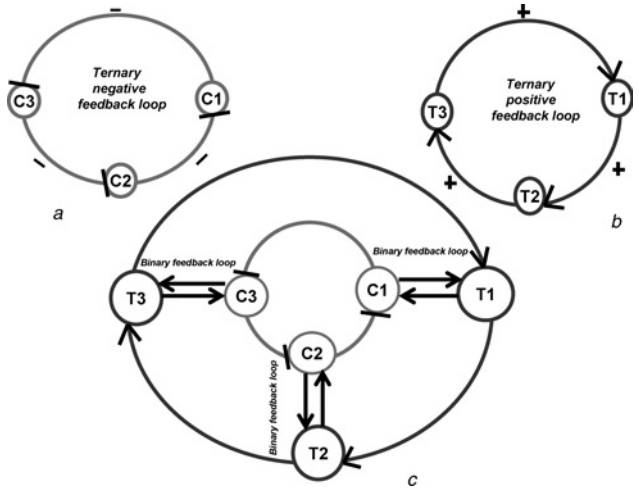

Fig. 2 *Regulatory networks of homogeneous and mixed feedback loops*

a In the top left panel is shown the homogeneous negative feedback loop circuit with only negative regulations that regulate the next one in a serial anti clockwise fashion
b In the right panel is shown the homogeneous positive feedback loop with only positive activators that regulate the next one in a serial clockwise fashion. The homogeneous feedback loops with three elements are called as 'ternary' feedback loops. T_1, T_2 and T_3 are the dynamical variables of the positive feedback loop denoted by '+'. C_1, C_2 and C_3 are the dynamical variables for the negative feedback loop denoted by '−'
c In the bottom panel, the ternary feedback loops linked by binary positive feedback loop with only positive regulations are shown by the black arrows

encountered in almost all the biological regulatory systems consists of both positive and negative feedback loops, for example, as in Fig. 1*c*. In this article, a different class of feedback loop abstracted from the interactions among the transcription factors, cyclins and their inhibitors of the budding yeast cell cycle is presented. The feedback loops are 'homogeneous', that is, positive feedback loop comprises only positive regulations and the negative feedback loop comprises only negative regulations. It can be noticed in Fig. 1*e* that the homogeneous negative feedback loops with only negative regulations cannot be realised from the two element feedback loop. Therefore the negative feedback loops with an odd number of elements (three elements) connected only by inhibitory interactions identical to the synthetic genetic network, repressilator (Fig. 2*a*) [5] is realised in budding yeast cell cycle by considering interactions among the cyclins and their inhibitors. Similar arrangement for the positive feedback loop with only positive regulations is constructed by abstracting the sequential regulation of the transcription factors from the chIP–chip data of the budding yeast cell cycle (Fig. 2*b*). The homogeneous feedback loops with three elements are termed 'ternary' feedback loops. Further, the corresponding elements of these homogeneous feedback loops are linked by the positive feedback loops with only positive regulations. These are termed 'binary' feedback loops. These interactions result in a 'non-homogeneous' or 'mixed' feedback loops (Fig. 2*c*). The orientation of the ternary homogeneous feedback loops are opposite to each other; that is, the homogeneous positive feedback loop has clockwise positive regulations, whereas homogeneous negative feedback loop has anticlockwise negative regulations.

1.1 Motivation and aim of the present study

In this section, the motivation behind the construction of the present network of topology from the experimental data is provided briefly. The details are given in a later section of the article. In budding yeast, the transcription factors regulate each other serially as determined from the chIP–chip data [17]. Applying redundancy criteria to the transcription factors that play a specific role in each phase of the cell cycle results in the ternary positive feedback loop as shown in Fig. 2*b*. The negative feedback loop with only negative regulation among the cyclin complexes Cln/Cdc28, Clb/Cdc28 and their inhibitor Sic1 are constructed from the minimal model of [18], which again is based on the experimental data (Fig. 2*a*). Finally, the interactions between the transcription factors, cyclin–cdk complexes and their inhibitors are taken mainly from [17]. Assembling of these interactions results in the mixed feedback loops (Fig. 2*c*). Therefore this topology is an abstraction from the experimental data and not artificially generated. To reduce the complexity of the model, finer details from the experiments are not incorporated in the present study, yet the bifurcation diagram is complex and exhibits many interesting dynamics. The positive feedback loop, because of the serial regulation of the transcription factors and the binary feedback loops results in a novel topology. This ternary positive feedback loop has not been considered in the minimal model of [18] or in the later rigorous models of [19, 20]. The present model can be considered as a subset of Tyson and Novak's minimal model to which the new information, namely the ternary positive feedback loop, is incorporated in the model.

Since this topology is novel, various dynamics exhibited by this network is initially presented. In particular, the influence of binary and ternary positive feedback loops that generates domino-like oscillations and the checkpoint mechanism are studied in detail by constructing one and two parameter bifurcation diagrams. The cell cycle and checkpoint dynamics of the budding yeast are presented in the latter part of the article. The article is organised in the following way. In the second section, the dynamics of ternary feedback loops linked with and without the binary positive feedback loops are studied in detail by

constructing one and two parameter bifurcation diagrams. The details of the construction of this novel topology in a modular form from the experimental data of budding yeast cell cycle and their dynamics are presented in the third and fourth sections. The final section contains the discussion, conclusion and the future direction of research. All the bifurcation diagrams are generated using the software XPPAUT [21] and the numerical simulations are carried out using MATLAB [22] and linear stability analysis using MATHEMATICA [23]. Since the concentration of most of the proteins are not known, we have taken the concentration of the dynamical variables in nanomolar (nM) and the time in minutes (min). All the dimension of the rates of the equations and the kinetic constants is given in Table 1 and taken to be standard values. For certain specific simulations the modification of the standard values are made and these are provided appropriately in the legend of the figures.

2 Dynamics of ternary homogeneous feedback loops

2.1 Bistability from the homogeneous positive feedback loop with only positive regulations

Ternary homogeneous positive feedback loops constructed with the dynamical variables T_1, T_2 and T_3, are sequentially regulated; dynamical variable T_1 positively regulates T_2 and in turn is regulated by T_3 as shown in the top-right panel of Fig. 2*b*. This regulatory network described by the Hills equations exhibits both hysteresis and bistability. The equations are

$$\frac{dT_1}{dt} = j_1 + \frac{\upsilon_{d_1} T_3^n}{k_{m_1}^n + T_3^n} - k_{d_1} T_1 \quad (1)$$

$$\frac{dT_2}{dt} = j_2 + \frac{\upsilon_{d_2} T_1^n}{k_{m_2}^n + T_1^n} - k_{d_2} T_2 \quad (2)$$

$$\frac{dT_3}{dt} = j_3 + \frac{\upsilon_{d_3} T_2^n}{k_{m_3}^n + T_2^n} - k_{d_3} T_3 \quad (3)$$

j_1, j_2, j_3 denote the basal rates, $\upsilon_{d_1},\upsilon_{d_2},\upsilon_{d_3}$ the rate of activation or the positive feedback strength, k_{m_1,m_2,m_3} the threshold constants, k_{d_1,d_2,d_3} the degradation constants and n the Hill's constant. For the choice of parameters given in Table 1, bistability and hysteresis (Fig. 3*a*) are observed with υ_{d_2} as the parameter. Linear stability analysis performed around the three steady states confirms the occurrence of bistability (shown in the Appendix). Robustness to the parameter variation is determined from the two parameter bifurcation diagram with j_1, k_{d_1} and υ_{d_1} as the dependent parameters and activation rate υ_{d_2} as the independent parameter. All the two parameter bifurcation diagrams exhibit cusp bifurcation that divides the monostable from the bistable region (Fig. 3*b*, *c*, *d*). The wide bistable regime indicates the robustness of the bistable system to the large parameter variations. Even though all the three parameters exhibits bistability for a wide range, υ_{d_1} operates at a much wider range than the basal and degradation rates. The scale of υ_{d_1} is different from the rest of the parameter plots in Fig. 3*d*.

Table 1: Parameter values used for mixed feedback loops, unless otherwise stated in the legend of the figures

Paramerer	Value used in the simulation
j_1	0.9 nM min^{-1}
j_2	0.6 nM min^{-1}
j_3	0.6 nM min^{-1}
υ_{d_1}	5.0 nM min^{-1}
υ_{d_2}	5.0 nM min^{-1}
υ_{d_3}	5.0 nM min^{-1}
k_{d_1}	0.9 min^{-1}
k_{d_2}	0.8 min^{-1}
k_{d_3}	0.8 min^{-1}
k_{c_1}	0.15 min^{-1}
k_{c_2}	0.15 min^{-1}
k_{c_3}	0.15 min^{-1}
k_{m_1}	5 nM
k_{m_2}	5 nM
k_{m_3}	5 nM
υ_{12}	15 nM min^{-1}
υ_{11}	15 nM min^{-1}
υ_{10}	15 nM min^{-1}
k_{120}	10 nM
k_{110}	10 nM
k_{100}	10 nM
k_{d_4}	0.16 min^{-1}
k_{d_5}	0.16 min^{-1}
k_{d_6}	0.16 min^{-1}
n	3.0

2.2 Oscillations from the homogeneous ternary negative feedback loop with only negative regulations

The dynamical variables C_1, C_2 and C_3 negatively regulate each other in an anticlockwise direction to give rise to homogeneous ternary negative feedback loop. C_1 negatively regulates C_3 and itself is negatively regulated by C_2 as shown in Fig. 2*a*. This topological arrangement of the negative feedback loop and the model described later are identical to the classical synthetic gene regulatory network, the repressilator; except that the present equations have no basal rate. The equations are

$$\frac{dC_1}{dt} = \frac{\upsilon_{12} k_{120}^n}{k_{120}^n + C_2^n} - k_{d_4} C_1 \quad (4)$$

$$\frac{dC_2}{dt} = \frac{\upsilon_{11} k_{110}^n}{k_{110}^n + C_3^n} - k_{d_5} C_2 \quad (5)$$

$$\frac{dC_3}{dt} = \frac{\upsilon_{10} k_{100}^n}{k_{100}^n + C_1^n} - k_{d_6} C_3 \quad (6)$$

In these equations, υ_{12}, υ_{11}, υ_{10} are the production rates, k_{120}, k_{110}, k_{100} are the threshold constants above which the inhibition takes place, k_{d_4,d_5,d_6} the degradation rates and n the Hill constant.

For appropriate choice of parameters given in Table 1, linear stability analysis confirms the occurrence of Hopf bifurcation (HB) (shown in Appendix). The HB is supercritical in nature where the unstable steady state surrounds the stable limit cycle (Fig. 4*a*). Oscillations are possible for the choice of parameters when the Hill's coefficient is

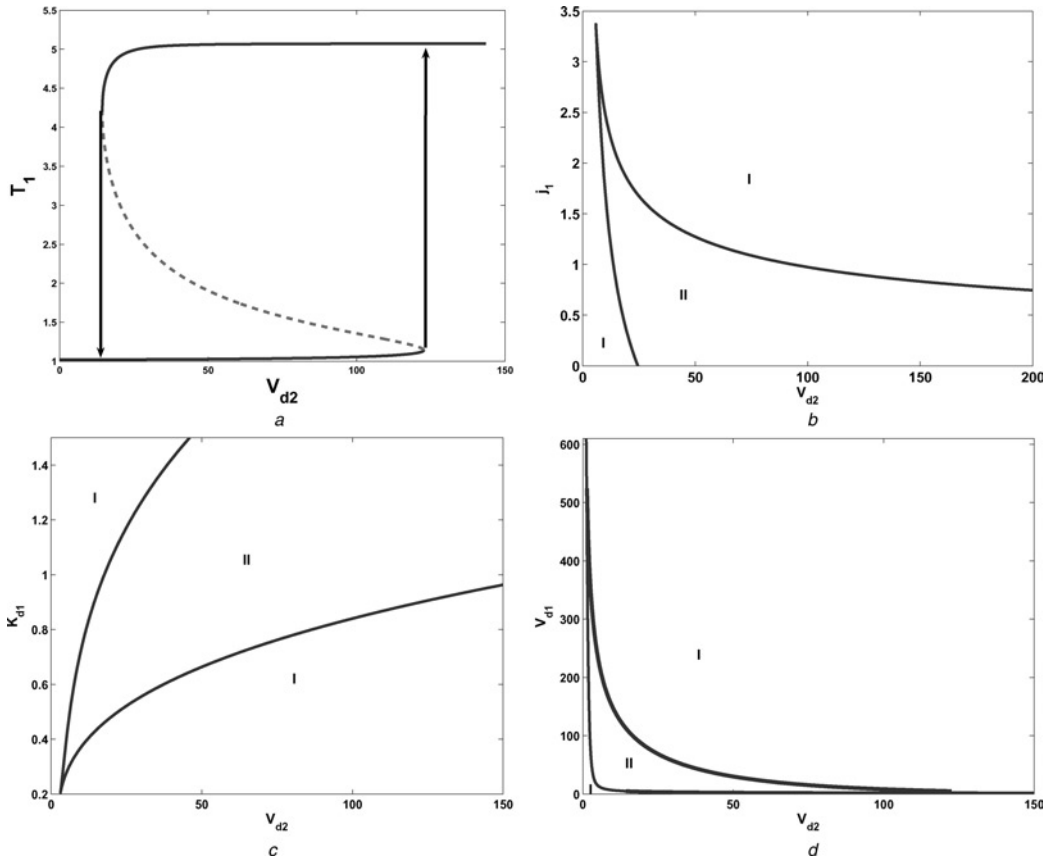

Fig. 3 *Occurrence of bistability and the two parameter bifurcation diagram for the positive feedback loop*

a Bifurcation diagram with υ_{d_2} as the bifurcation parameter for (1)–(3). Continuous lines are the stable steady state, whereas the dashed lines are the unstable steady state. Bistability can also be obtained for υ_{d_1}, υ_{d_3}, j_1, j_2, j_3 for an appropriate parameter set

b, *c* and *d* are the two parameter bifurcation diagrams that generates cusp point. Region of monostabilty (I) and bistability (II) is identified for three different parameters with respect to the parameter υ_{d_2}

b is the bifurcation diagram for the basal rate j_1, whereas *c* and *d* are for υ_{d_1}, the feedback strength and k_{d_1} the degradation constant, respectively

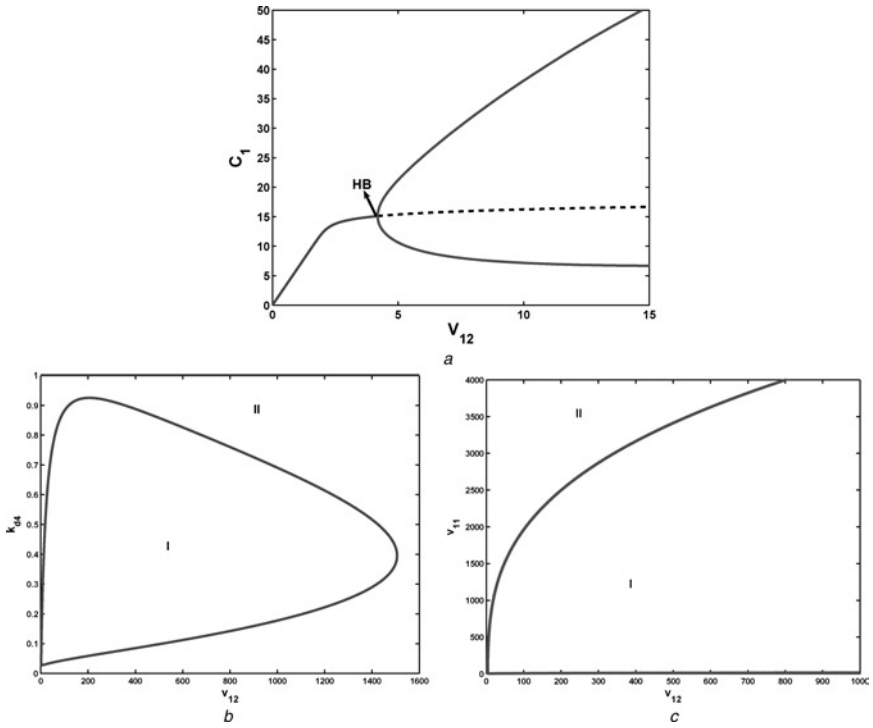

Fig. 4 *Occurrence of supercritical Hopf bifurcation and the two parameter bifurcation diagram for the negative feedback loop*

a Bifurcation diagram for (4)–(6) with υ_{12} as the bifurcation parameter. Continuous lines are stable steady state and filled circles are the stable limit cycle oscillations. The supercritical Hopf bifurcation denoted by HB surrounds the unstable steady state shown as darked lines. Supercritical Hopf bifurcation can also be obtained for υ_{11}, and υ_{10} for an appropriate parameter set

b and *c* Two parameter plane diagram for υ_{11}, and k_{d_4}. I and II are the region of oscillation and the stable steady state, respectively, separated by the dark lines

greater than 2 (shown in Appendix). Two parameter bifurcation diagram constructed for the parameters v_{11} and k_{d_4} with v_{12} as an independent parameter separates the wide wide regime of oscillations from the stable steady state (Figs. 4*b*, *c*). This indicates the robustness of the oscillatory system to a large parameter variations. Similar bifurcation diagram constructed for the other parameters have also found to exhibit oscillations to a wide range of values (bifurcation diagram not shown).

In summary, homogeneous positive feedback loop exhibits bistability and negative feedback loop exhibits HB. The dynamics are robust to large parameter variations and are in the biologically plausible range. These values are partially modified to understand the general dynamics of the whole system and that of the budding yeast cell cycle.

2.3 Dynamics of the ternary positive and negative feedback loops linked by the binary positive feedback loops

Ternary homogeneous positive and negative feedback loops described in the earlier two sub-sections are linked by the homogeneous binary positive feedback loops with only positive regulations. This is shown by the black arrows in the bottom panel of Fig. 2*c*. By coupling, the whole egulatory network becomes 'non-homogeneous', that is, the network consists of mixed feedback loops. Mathematically, the coupling of two homogeneous feedback loops can be expressed either by the linear or nonlinear terms. To generate interesting dynamics, coupling of C's to T's are described by the linear equations, whereas that of T's to C's are described by the nonlinear equations as in the following

$$\frac{dT_1}{dt} = j_1 + \frac{v_{d_1} T_3^n}{k_{m_1}^n + T_3^n} + \boldsymbol{k_{c_1}} \boldsymbol{C_1} - k_{d_1} T_1 \tag{7}$$

$$\frac{dT_2}{dt} = j_2 + \frac{v_{d_2} T_1^n}{k_{m_2}^n + T_1^n} + \boldsymbol{k_{c_2}} \boldsymbol{C_2} - k_{d_2} T_2 \tag{8}$$

$$\frac{dT_3}{dt} = j_3 + \frac{v_{d_3} T_2^n}{k_{m_3}^n + T_2^n} + \boldsymbol{k_{c_3}} \boldsymbol{C_3} - k_{d_3} T_3 \tag{9}$$

$$\frac{dC_1}{dt} = \frac{v_{12} \boldsymbol{T_1^n}}{k_{120}^n + \boldsymbol{T_1^n} + C_2^n} - k_{d_4} C_1 \tag{10}$$

$$\frac{dC_2}{dt} = \frac{v_{11} \boldsymbol{T_2^n}}{k_{110}^n + \boldsymbol{T_2^n} + C_3^n} - k_{d_5} C_2 \tag{11}$$

$$\frac{dC_3}{dt} = \frac{v_{10} \boldsymbol{T_3^n}}{k_{100}^n + \boldsymbol{T_3^n} + C_1^n} - k_{d_6} C_3 \tag{12}$$

All the newly added coupling terms in the equations are indicated in the bold. The linear coefficients k_{c1}, k_{c2}, k_{c3} in the (7)–(9) denotes the positive influence of C's on T's. On the other hand, the positive influence exerted by T's on C's as in (10)–(12) are highly nonlinear. To determine the effect of coupling on the dynamics of the system, one parameter bifurcation diagram is constructed for (7)–(12) with v_{d_2} as the parameter. Four distinct dynamical features are observed.

1. The mixed feedback loop exhibits both bistability and supercritical HB (unstable steady state surrounded by a stable limit cycle) suggesting the influence of both ternary positive and negative homogeneous positive feedback loop brought about by the binary positive feedback loops in the system. The stable limit cycle undergoes secondary Hopf bifurcation (SB) to give rise to unstable limit cycle that (inset of Fig. 5*b*) terminates with infinite period. There is also an unstable oscillation that emerges from the saddle and terminates with large amplitude and infinite period indicating saddle-loop (SL) bifurcation. These are homoclinic bifurcation with period tending to infinity (inset, Fig. 5*c*).

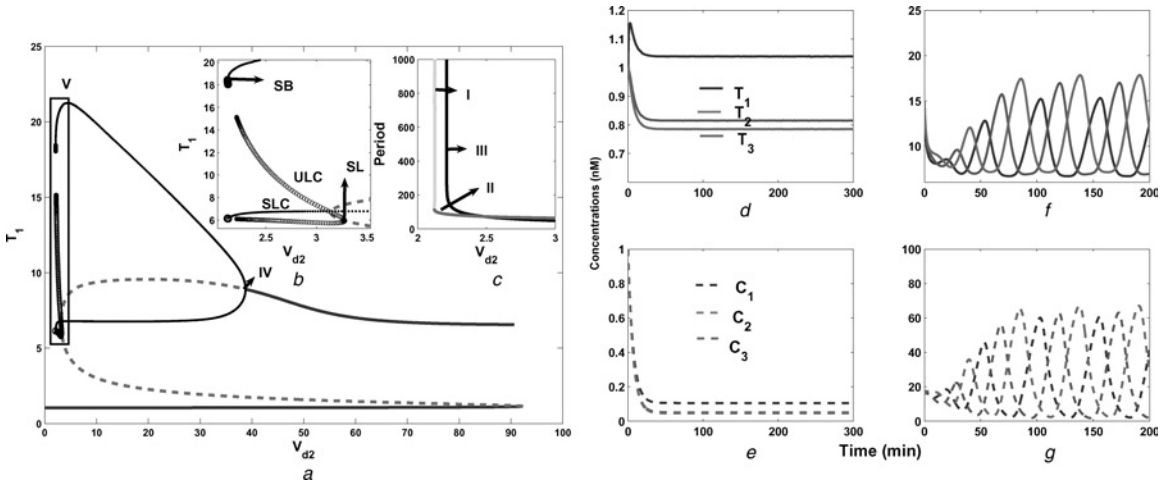

Fig. 5 *Influence of linking the corresponding elements of the homogeneous ternary feedback loops by the binary feedback loops*

a One parameter bifurcation diagram with v_{d_2} as the bifurcation parameter is shown. Continuous lines are the stable steady states and the dashed lines are the unstable steady states. The filled circles are the maximum and minimum amplitude of the limit cycle oscillations. The unfilled black circle is the unstable limit cycle

The inset *b* is the enlarged portion of the rectangle V. Stable limit cycle (SLC) oscillations emerge from the supercritical HB IV, which further undergoes SB to give rise to unstable limit cycle oscillations. This collides with saddle node with an infinite period. Unstable limit cycle (ULC) oscillations emerges from the saddle and terminates with a large amplitude and infinite period. This is the SL bifurcation

In inset *c* is shown the period of the oscillations. II is the period of the stable oscillations that emerges from A whereas I is the period of the unstable oscillations that results from the SB. The period of the oscillations tends to infinity suggesting homoclinic bifurcation

In the right panel the time series for two different initial conditions are shown

d and *e* are the time series of T's and C's respectively, for initial condition [1, 1, 1, 1, 1, 1]

f and *g* are the time series for initial conditions [15, 15, 15, 15, 15, 15] that exhibits domino-like oscillations

2. Oscillations which are absent in T's, are induced by C's through linear and nonlinear coupling.
3. The dynamics of the system are dependent on the initial conditions of the system (Figs. 5*d*, *e*, *f* and *g*). Depending on the initial conditions the system settles down either to the oscillatory or to the stable steady state.

To obtain a better insight about the influence of binary positive feedback loop in the system, two parameter bifurcation diagram is constructed with υ_{d_2} and k_{c_1} as the parameters (Fig. 6*a*). The highlights of the two parameter bifurcation diagram are

(i) Two types of limit cycle oscillations are observed in the system: sinusoidal and relaxation-like oscillations (regions I and II, respectively, in Fig. 6*a*) because of the influence of the binary feedback loops. To distinguish these two types of limit cycle oscillations, one parameter bifurcation diagram is constructed with k_{c_1} as the parameter for a constant $\upsilon_{d_2} = 5$ (shown in Fig. 6*d*). For a low value of k_{c_1}, smooth unstable oscillations (ring type) arise from the Hopf bifurcation (IV, inset of Fig. 6*d*). This unstable oscillation from the saddle changes its stability (V, inset of Fig. 6*d*) to give rise to stable limit cycle that collides with stable node with infinite period. The collision occurs at a high value of k_{c_1} and exhibits relaxation oscillations with a high period. This is saddle-node bifurcation with an Infinite PERiod (SNIPER). Broadly, the transitions in the two parameter bifurcation diagram in Fig. 6*a* when moving from the bottom (low k_{c_1} and υ_{d_2}) to top (high k_{c_1} and low υ_{d_2}) are (a) region III $\rightarrow$ I is the transition from the stable steady state to HB and (b) region I $\rightarrow$ II is the transition from stable limit cycle oscillations to SNIPER bifurcation through a SB. In the region of low k_{c_1}, smooth ring type oscillations are observed because the negative feedback loop dominates over the positive feedback. In the region of high k_{c_1}, relaxation oscillations are observed because of the strong influence exerted by the binary positive feedback loop over the negative feedback loop. There are also a small region of cusp and Takens-Bogodonov (TB) bifurcations in the two parameter bifurcation diagram that occurs in between regions III and I. Cusp bifurcation arises because of the confluence of three steady states of the saddle-node to a point (C_1 and C_2 of Fig. 6*b*) and TB bifurcation (TB in Fig. 6*b*) arises because of the collision of Hopf point with the saddle-node bifurcation [24].
(ii) The oscillations are arrested immediately when the binary positive feedback loop is silenced. This is effected by reducing the coupling constants k_{c_1}, k_{c_2}, k_{c_3} to zero independently. The oscillations are not resumed even after the coupling constants are restored to its original value after some time. One such case is shown in the Figs. 7*a* and *b*. This is because the dynamical variables are moved away

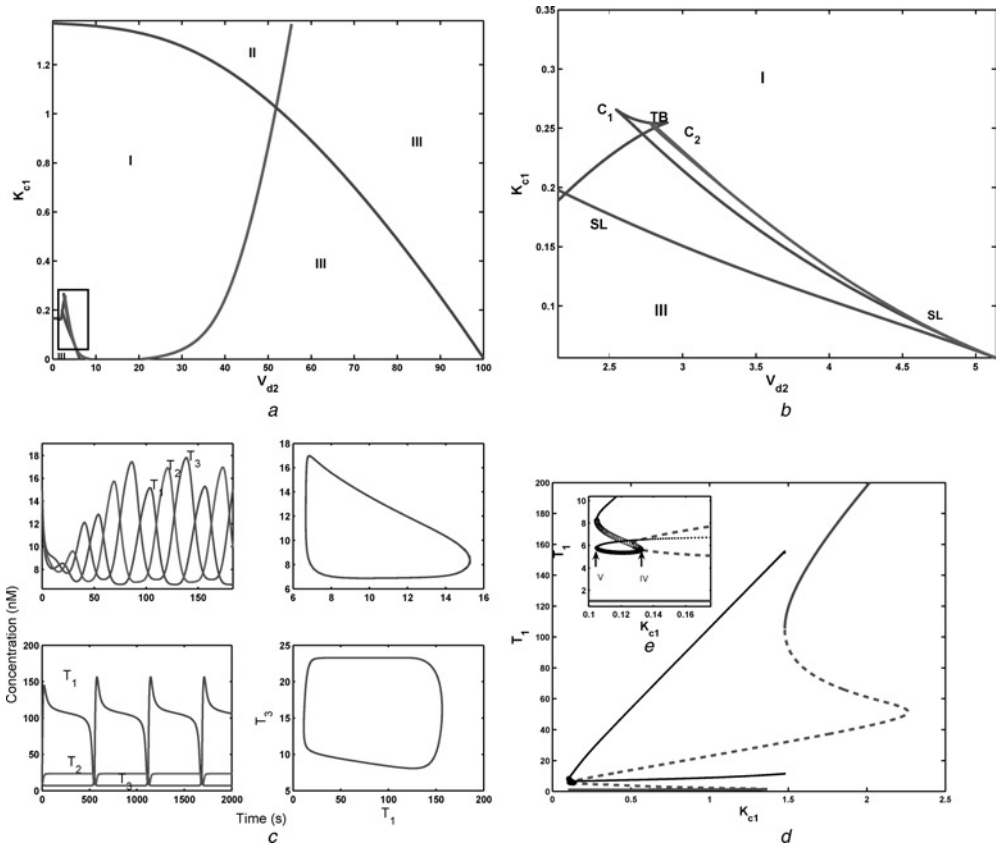

Fig. 6 *Two parameter bifurcation diagram illustrating the influence of binary positive feedback loop*

a Two parameter bifurcation diagram of the model (7)–(12) with υ_{d_2} and k_{c_1} as the parameter is shown. There are three regimes with I and II being the regime of smooth sinusoidal (ring type) and relaxation-like oscillations, respectively. III is the stable-steady state regime
In *b* is shown the two cusp bifurcation (C_1 and C_2) and TB is the Takens-Bogodonov bifurcation and SL is the saddle-loop bifurcation enlarged from the rectangular box in *a*. See the text for explanation. Regimes of smooth domino-like oscillations (I) that are separated from relaxation oscillations (II) are shown for a particular coupling constant
c Time series and their corresponding attractors for $k_{c_1} = 0.15$ chosen from regime I that shows smooth oscillations and below time series and corresponding attractor for $k_{c_1} = 1.5$ chosen from regime II that shows relaxation oscillations. $\upsilon_{d_2} = 5$ is chosen for the simulation of time series
d One parameter bifurcation to illustrate the occurrence of smooth and relaxation oscillations and the inset *e* shows the starting of unstable limit cycle oscillations from saddle (IV) that changes it stability at (V) to stable limit cycle oscillations (see text for further explanations)

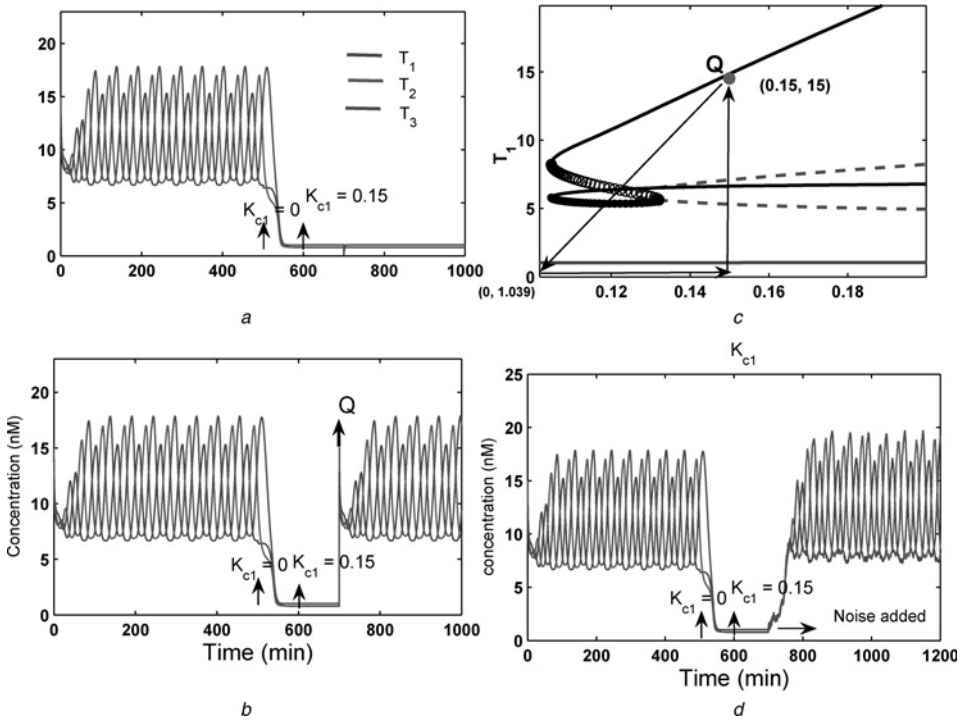

Fig. 7 *Effect of silencing the binary positive feedback loop and checkpoint-like mechanism*

a Complete arrest of oscillations when the coupling constant k_{c_1} is made zero at $t = 500$ for $\upsilon_{d^2} = 5$. The oscillations did not resume even after the coupling constant $k_{c_1} = 0.15$ is restored to its original value at $t = 600$
The rest of the parameter values are the same

b Initiation of oscillations when the initial concentrations are reset to [15, 15, 15, 15, 15, 15] at $t = 700$ with $k_{c_1} = 0.15$. This is denoted by Q in the figure at $t = 700$

c One parameter bifurcation diagram from Fig. 6*d* is used to illustrate this behaviour. The triangle denotes the movement of the system when the parameter and concentration are reset. Starting from Q, which is same as in *b*, is the initial value of k_{c_1} and T where oscillations occur (0.15, 15). When k_{c_1} is made zero, the system moves to another stable steady state at (0, 0.5). When k_{c_1} is restored to its original value, the system is moved to another regime in the bifurcation diagram (0.15, 0.5) which again is the stable steady state. Finally when the concentration are reset the system moves to Q again and oscillation resumes.

d Oscillations resume when uniformly distributed random number with noise intensity of 0.07 is added (shown as horizontal arrow) to the stable steady state. The initial condition chosen for the simulation other than the noise induced oscillation is [15, 15, 15, 15, 15, 15]

from the limit cycle regime to the stable steady state in the phase space. The oscillations can be restored by two different ways: (a) by changing the initial conditions and (b) by adding a small percentage of noise to stable steady state of the system provides information about the robustness of the steady state. In case (a), the oscillations are restored when the concentration of the dynamical variables are reset above the threshold value of both the bistable and oscillatory regime. This is illustrated using bifurcation diagram shown in Fig. 7*c*. This brings in the notion of checkpoint in the model. In case (b), the stable system obtained is not robust when the stable steady states are perturbed with a small percentage of noise as the noise induces a transition from stable steady state to oscillations (Fig. 7*d*). This is simulated using uniformly generated random number in MATLAB with a noise intensity of 0.07 added to the stable steady state concentration restores the oscillations, suggesting the sensitive nature of the system to molecular noise. A detailed work on the role of molecular noise will be taken up as a future task.

(iii) When the Hill's coefficient is changed from $n = 3$ to $n = 2$ (Fig. 8*a*), the bifurcation diagram becomes less complex because of the separation of bistable regime from the two supercritical HB. Most importantly, homogeneous negative feedback loop alone do not exhibit HB for $n = 2$, that is, oscillation is absent for the parameter set chosen (shown in the Appendix). This clearly indicates the role of homogeneous positive feedback loop in inducing and amplifying the oscillations in the system. This result is similar to the experimental results of [25] wherein their experiments on *Xenopus laevis* produced damped oscillations when the positive feedback loop is silenced. A summary of changing Hill's coefficient and the corresponding dynamics in the presence and absence of coupling the ternary feedback loops observed in the bifurcation diagram is given in Table 2.

3 Details of the construction of the mixed feedback loop from the budding yeast cell cycle data

In normal eukaryotic cell cycle, both positive and negative feedback loops guide the cell through various phases, namely G1, S-G2 and M phases [26]. In budding yeast cell cycle, these feedback regulations are carried out by cyclin-dependent kinase (CDK) along with two families of cyclins, Cln's and Clb's and the inhibitors of the cyclin-dependent complexes [27, 28]. Cyclins themselves are controlled by various transcription factors through the positive feedback loops at different phases of the cell cycle [29–31]. The checkpoints, which are discussed at length in the later part of the article, involves the activation and suppression of transcription factors, cyclins and their inhibitors through silencing specific feedback loops. In general, the precise events in the cell division cycle are controlled by the transcription factors (TF), Cyclin/Cdk's and their inhibitors through intricate feedback loops at different phases of the cell cycle. It is shown later that the complex interactions among the regulatory proteins of the budding

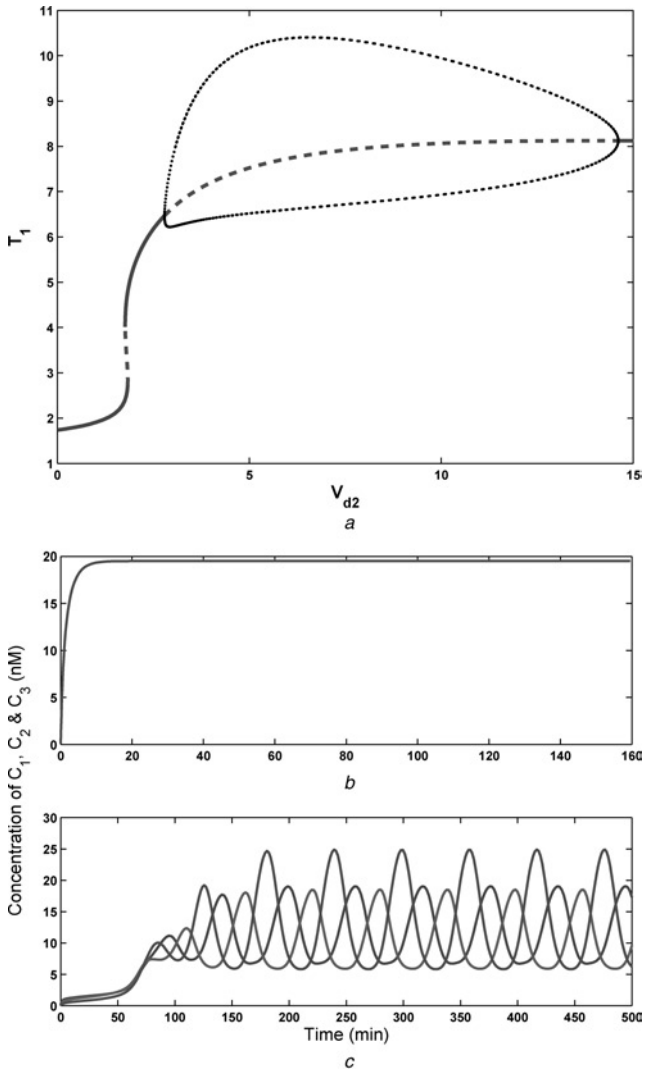

Fig. 8 *Effect of varying Hill's coefficient in the model*

a One parameter bi furcation diagram is constructed for Hill's coefficient $n = 2$ and $v_{d_2} = 4$, keeping the other parameters constant. The bifurcation diagram has isolated saddle-node and HB regime that do not overlap. There are two supercritical HB in the diagram
In *b* Oscillations are absent for $n = 2$, in the absence of both ternary and binary positive feedback loops and *c* Oscillations are induced and amplified in the presence of both binary and ternary positive feedback

yeast cell cycle can be segregated into two ternary feedback loops as shown in Fig. 2*a* and *b*. The basis for the segregation based on the experimental data is presented in the following two sections in detail.

3.1 Construction of homogenous ternary positive feedback loop from the sequential regulation of TFs

Recently, through genome-wide location analysis the cell cycle specific TFs functioning at one phase was found to positively regulate the transcription factors in the subsequent phase [17, 32]. These are two complexes, Mbp1 and Swi6 (hereafter called MBF) and the complex of Swi4 and Swi6 (hereafter called SBF) that control late G1 genes. The transcription factors Mcm1, Fkh1, Fkh2 and Ndd1 control the late G2/S genes whereas Swi5 and Ace2 regulate both late M and early G1 genes. Mcm1 is also involved in the transcription of M/G1 genes. The sequential regulation of TFs are as follows: The cycle starts with the late G1 transcription factors SBF and MBF that regulate Ndd1 a G2 gene. Ndd1 positively regulates Mcm1 and Fkh2 genes that are important for G2/M transition. Further, Ndd1 together with Mcm1/Fkh2 regulates Swi5 and Ace2. Swi5/Ace2/Mcm1 activates M/G1 genes, completing one full cycle.

Homogeneous positive feedback loop is obtained from the TF's that are clubbed together because of their high functional redundancies [17]. In G1 phase, the transcription factors SBF, and MBF, respectively, share 31% and 77% identity in their DNA binding domains, that is,

$$\mathrm{SBF} + \mathrm{MBF} \rightarrow \mathrm{T}_1$$

In S-G2 phase, Fkh1 and Fkh2 are 16% identical and mutations in Mcm1 and Ndd1 are lethal. Therefore all the four transcription factors are taken as one dynamical variable as T_2, that is

$$\mathrm{Fkh1} + \mathrm{Fkh2} + \mathrm{Ndd1} + \mathrm{Mcm1} \rightarrow \mathrm{T}_2$$

In M-phase Swi5 and Ace2 are 17% identical and taken together as one dynamical variable T_3, that is

$$\mathrm{Swi5} + \mathrm{Ace2} \rightarrow \mathrm{T}_3$$

The wiring of the homogeneous positive feedback loops that involves only TFs as shown in Figs. 9*a* and *b* are same as in Fig. 2*b*. The mathematical equations (1)–(3) are taken for the analysis and this gives rise only to bistability.

3.2 Construction of homogeneous ternary negative feedback loop from the cyclins and their inhibitors

Cyclins and their inhibitors provide negative feedback loop in the model. Two different Cyclins, Cln's and Clb's

Table 2: Effect of varying Hills coefficient '*n*' in the bifurcation diagram

Hill's coefficient (*n*)	Uncoupled system eqns (1)–(3)(+FBL)	eqns(4)–(6)(−FBL)	Coupled system eqns (7)–(12)
1	SS	SS	SS
2	SN	SS	HB(SUP + SUP) + SN
3	SN	HB	HB(SUB + SUP) + SN
4	SN	HB	HB(SUB + SUP) + SN
5	SN	HB	HB(SUB + SUP) + SN

The effect of '*n*' on the dynamics of both coupled and uncoupled feedback loops are shown. The notation used are SS, steady state; SN, saddle node; HB, Hopf bifurcation; SUP, supercritical and SUB, subcritical Hopf bifurcations; FBL, feedback loop. For $n = 2$, Hopf bifurcation is not seen in the negative feedback loop of the uncoupled system. But Hopf bifurcation is obtained when coupled for certain values of parameter. This is shown in Fig. 7. When *n* increases, the regime of steady state increases, whereas the regime of Hopf bifurcation decreases

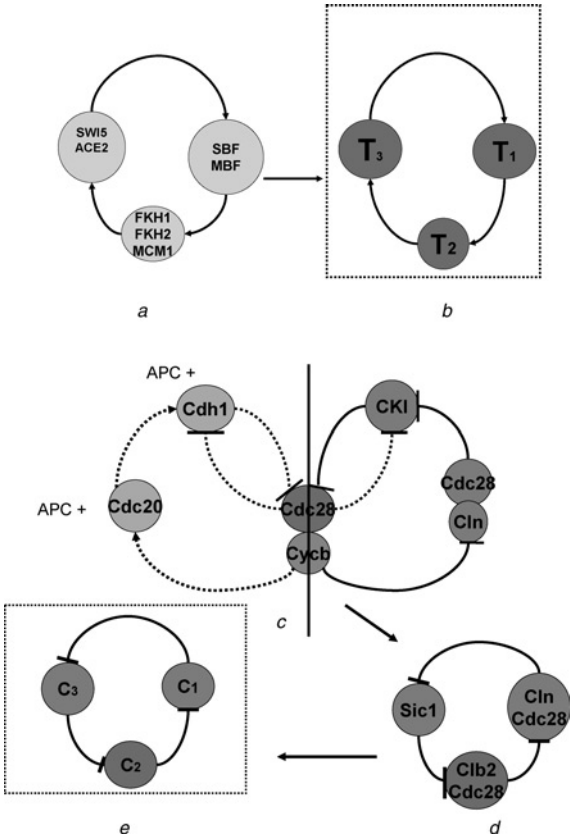

Fig. 9 *Abstraction of wiring diagram for the cell cycle of budding yeast for the present study*

Two different positive regulations are shown. The serial positive regulation of only TFs is shown in *a* and *b*

The negative regulations are shown in *c*, *d* and *e*. In negative feedback loop, CKI in *c* is replaced by Sic1 in *d*

Also the negative regulations shown in dashed arrow has not been taken into consideration for the construction of feedback loop similar to represillator in the present study

The circuits *b* and *e* are the positive and negative feedback loops that are same as the one shown in Figs. 2*b* and 2*a*, respectively

together with CDK Cdc28, play an important role at the appropriate phases of the cell division cycle. The complex of Cdc28 and Cln3 triggers the cell cycle and the complex of Cdc28–Cln2, Cdc28–Clb5 and Cdc28–Clb2 initiates budding, DNA synthesis and mitosis, respectively. The inhibitors of the cyclins are Sic1, Cdh1 and Cdc20 that down-regulate Cdc28–Clb2 [33, 34].

Constructing wiring diagram for the cyclins and their inhibitors similar to the TFs is not a trivial task. This is particulary true in the case of mitotic exit, where APC–Cdc20, APC–Cdh1 and Sic1 involve in the inhibition of Clb2–Cdc28 complex. APC–Cdc20 and APC–Cdh1 takes a different path, whereas Sic1 takes another path in down-regulating Clb2–Cdc28 complex. Their role in the mitotic exit is also different. To overcome this problem, we consider the circuit diagram of [18]. The circuit diagram shown in Fig. 9*c* is similar to the circuit diagram shown in Fig. 6 of [18]. In the circuit diagram, cyclins Clns and Clbs complexed to the kinase Cdc28 pushes the cell to various phases of the cell cycle. Clb–Cdc28 is required to START cell cycle with the help of Cln/cdc28, whereas to FINISH the cell cycle, Clb–Cdc28 is removed by the inhibitors of cyclins APC–Cdc20, APC–Cdh1 and Sic1.

To START the cell cycle, Cln–Cdc28 kinases that are immune to inhibitors, eliminate Sic1 by phoshorylating it [27]. This releases Clb–Cdc28 from the clutch of inhibitors to start the cell cycle. Once the cell cycle is started, Cln–cdc28 is inhibited by the Clb–cdc28 complex.

In the FINISH transition, the two important inhibitors Cdh1 and Sic1 binds to Clb2–Cdc28 complex and inhibits its activity. In the current study, out of the two paths shown in Fig. 9*c* from [18], only the Clb–cdc28, Cln–cdc28 and Sic1 are taken, whereas the other pathway is excluded. Thus the negative regulation Clb–cdc28, ⊣ cln–cdc28 ⊣ Sic1 ⊣ Clb/cdc28 constitutes a negative feedback loop identical to the repressilator.

The wiring of homogeneous negative feedback loop that involves only cyclin and their inhibitors is same as the wiring diagram as in Fig. 2*a* and the mathematical equations (4)–(6) describing this process is considered. This gives rise only to limit cycle oscillations.

3.3 Mutual interaction between the TFs, the cyclins and their inhibitors: Generation of mixed feedback loops

The circuit diagram for the coupling of TFs, cyclins and their inhibitors are constructed by taking the following facts into consideration (Fig. 10).

In G1 phase, expression of Cln's (except Cln3) are positively controlled by SBF. SBF in turn is positively controlled by all Clns as well as Clb5 [35, 36] (Fig. 10*a*). Cyclins 1 and 2 are clubbed to Cln as shown in Fig. 10*a*.

In S-G2-M phase Clb2 is autocatalytic, because Clb2 activates its own TFs (MCM1) [31, 37]. Therefore the mutual activation of Clb2 and MCM1 are considered in the circuit (Fig. 10*b*).

In M-G1 phase, Sic1 transcription is regulated by Swi5 [38] But the inhibitor Sic1 has indirect influence on the transcription factor SWI5 by negatively regulating Clb2–Cdc28 complex that in turn down-regulates the production of SWI5. Since this is not a direct regulation it is shown in the dotted lines that completes the positive feedback loop (Fig. 10*c*).

In summary, the transcription factors T_1 regulates C_1 positively and vice versa in the G1-phase. In the S-G2-M phase transcription of Clb2 is autocatalytic and activates its own TF Mcm1/Fkh2/Ndd1. Also in this phase, T_2 regulates C_2 positively and vice versa. In M/G1 transition, Sic1 is regulated by Swi5. Sic1 has indirect influence on the TF Swi5. So the interaction between all the T's and C's are positively regulated in our model. The coupling of ternary positive and negative feedback loops through homogeneous binary positive feedback loops shown in the bottom panel of Fig. 2*c* gives rise to mixed feedback loops. The mathematical equations (7)–(12) are used to construct bifurcation diagrams to explain the dynamics of the cell division cycle.

4 Dynamics of the cell cycle network: Bifurcation diagrams and the cell cycle events

The dynamics of the budding yeast cell cycle is studied by taking υ_{d_2} as the control parameter. This parameter monitors the cell cycle growth and division as shown in the bifurcation diagram of Fig. 10. Importantly, the bifurcation diagram is used to illustrate the occurrence of domino-like oscillations and checkpoint dynamics. A rich bifurcation diagram illustrates the functioning of the cell cycle in terms of dynamical system theory. In budding yeast, there is no clear G2 phase and therefore can be considered as an alternation between G1 and S-G2-M phases [18, 39]. These phases of budding yeast cell cycle can be realised when υ_{d_2} changes from smaller to larger values. G1 is a stable steady state whereas S-G2-M phase is an unstable steady state surrounded by a

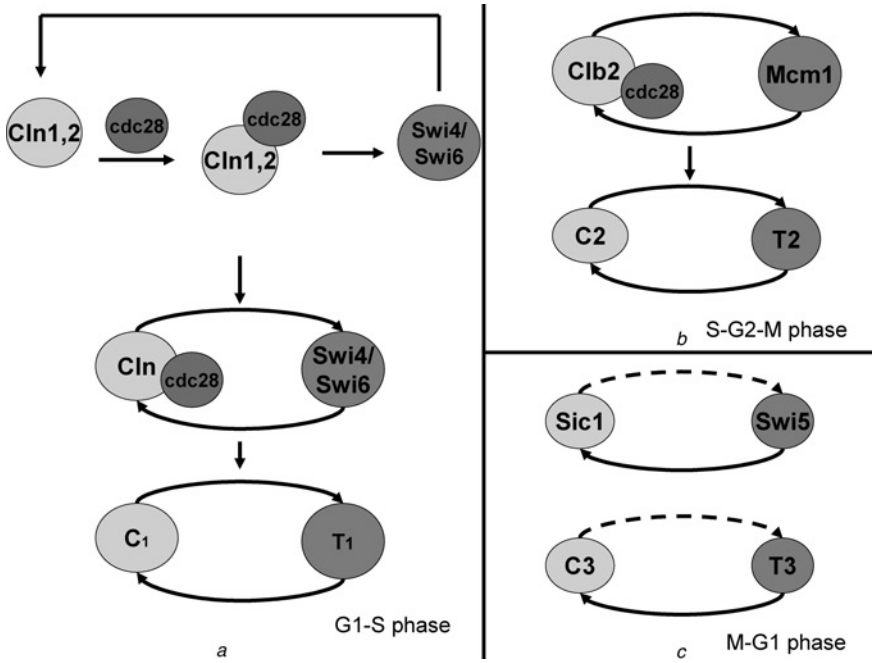

Fig. 10 *Abstraction of the relationship between TFs and the cyclins*

All the TFs regulate the cyclin–cdc28 complex positively. The cyclins also in turn regulate the TFs positively thus closing the positive feedback loop *a*, *b*

The TFs Swi5 in M-G1 phase shown in *c* regulate the inhibitor Sic1 positively, but not vice versa. The regulation of Swi5 by Sic1 is indirect and this is denoted by the dashed lines

T_1, T_2 and T_3 are the TFs, whereas C_1, C_2 are cyclin complexes and C_3 is the inhibitors of cyclins. The negative regulation of Sic1 by Clb2/cdc28 is not considered

stable limit cycle. There is also another stable steady state between these two phases that is very small and cannot be stabilised for a long time (shown as I in the bottom left panel of Fig. 11*a*). This is also the case in the budding yeast cell cycle. So to explain the dynamics of budding yeast cell cycle, this small steady state is not considered. Four saddle-node bifurcations at $\upsilon_{d_2} = 0.5769$, 0.5188, 0.6835, 0.4234 and three HBs at $\upsilon_{d_2} = 0.6831$, 0.5666 and 25.37 (I, II and III, respectively, in Fig. 11*b* and *c*) are observed. When υ_{d_2} is decreased slowly from a high value stable steady state is replaced by unstable steady state and supercritical HB at $\upsilon^H_{d_2} = 25.37$. When υ_{d_2} is further decreased, the period of the oscillations remains almost constant with the amplitude of the oscillations in proportion to $\sqrt{(\upsilon^H_{d_2} - \upsilon_{d_2})}$ (Fig. 11*d*). As υ_{d_2} is further decreased to a very low value, the period of the oscillation increases rapidly and the oscillatory solution disappears at $\upsilon_{d_2} = 0.7169$. This is the saddle node bifurcation with an Infinite PERiod [SNIPER; also called saddle node on invariant circle (SNIC)], where the stable limit cycle with finite amplitude disappears as the period diverges to infinity and is replaced by the stable node (shown in Fig. 11*a*). The system exhibits domino-like oscillations in a stepwise fashion (Fig. 12*a* and *b*) with a period of approximately 90 min in one cycle for υ_{d_2} being 1.052. This value is chosen for the simulation where the cell cycle is in unstable state surrounded by stable limit cycle; that is, in S-G2-M phase. The HBs at $\upsilon_{d_2} = 0.6831$, 0.5661, shown in Fig. 11*c* as I and II, is encompassed by the stable limit cycle oscillation emerged from the HB III (shown in Fig. 11*b*). A small region denoted by 'I' is an inverse supercritical HB from which the limit cycle oscillations undergo a cascade of period-doubling oscillations. II is a HB that emerges from large period and collides with the unstable steady state to give rise to SL bifurcation. This also terminates with an infinite period indicating SL bifurcation. Only HB III has physical significance in the model.

4.1 Explanation for the occurrence of domino-like oscillations

The bifurcation diagram (Fig. 11) and time series (Fig. 12) are used to explain the occurrence of domino-like oscillations in terms of Clb2 protein concentrations, that is, C_2 in the model. The concentration of C_2 can be either low or high depending on the phase in which the cell is present. This corresponds to either a stable steady state or an oscillatory state in the bifurcation diagram. At G1, the concentration of Clb2 is very low because the inhibitors of Clb2 namely Sic1 is in abundance, that is, C_3 is in abundance. This is a stable steady state in the bifurcation diagram. In other words, when the inhibitor Sic1 is high, Clb2 is low. Therefore there is an anti-phase relationship between C_2 and C_3 in the time series. But Cln's present in the G1 phase are immune to these inhibitors. When the concentrations of Cln's increases, that is, when C_1 crosses a threshold concentration, the inhibitor Sic1 is destroyed leading to an increase of Clb2 concentration followed by the transition from G1 to S-G2-M phase. In the bifurcation diagram this corresponds to a transition from the stable steady state (G1) to oscillatory state (S-G2-M). In S-G2-M phase, Clb2 is activated by the TF, T_2. Concomitantly, when Clb2 reaches a threshold concentration, it involves in an indirect negative regulation of the TFs in the G1 phase through the negative regulation of Clns. This results in the fall of concentration in both T_1 and C_1 and a simultaneous rise in the concentration of both T_2 and C_2. Therefore in S-G2-M phase, T_2 and C_2 are in phase with each other but out of phase with T_1 and C_1. In addition, at M-G1 phase, highly active Clb2 triggers their inhibitors. The inhibitor C_3 starts dominating at M-G1 transition and

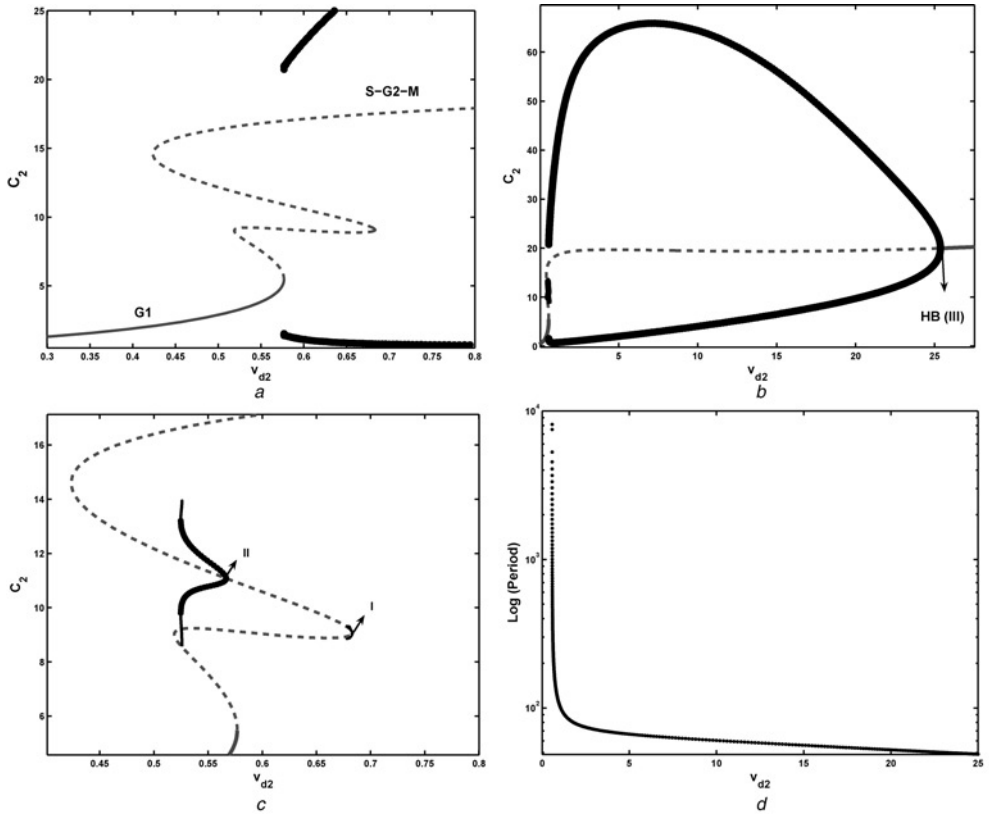

Fig. 11 *One parameter bifurcation diagram for cell division cycle of budding yeast*

One parameter bifurcation diagram is constructed with υ_{d_2} as the parameter. The other parameters that differs from the parameter set given in Table 1 are $j_2 = 0.5$, $j_3 = 0.2$, $k_{c_1} = 0.2$ $k_{c_2} = 0.22$, $k_{c_3} = 0.6$, $\upsilon_{d_1} = 6$, $\upsilon_{d_3} = 3$ and $n = 2$. I and II are the HB that takes place on the saddle and III is the supercritical HB

a G1 is the stable steady state shown by the thick lines, whereas S-G2-M state is an unstable steady state surrounded by the stable limit cycle that arise from HB III. In between these two states there is a small region of stable steady state that is not stabilised for a long time and this stable steady state is not considered for the budding yeast cell cycle dynamics. The limit cycle is shown in the dark black filled circle

In *b* complete bifurcation diagram is shown. The stable steady states are denoted by solid lines, unstable steady states by broken lines, stable limit cycle by filled circle and unstable limit cycle by unfilled circle

In *c* two other HB points (I and II) are shown. I and II are saddle loop bifurcation

In *d* is shown the period of the limit cycle arising from the HB III, which collides with the saddle and node namely saddle node on invariant circle. The period near this bifurcation blows to infinity suggesting the homoclinic nature of bifurcations

degrades Clb2 for the successful completion of one cell division cycle. In this phase T_3 and C_3 are in phase with each other but out of phase with T_2 and C_2. Simultaneously, C_1, which is immune to the inhibitors, initiates the next cycle by activating T_1. These events result in a domino-like oscillations because of highly ordered step-wise activation and destruction of the TFs, cyclins and their inhibitors at different phases of the cell cycle.

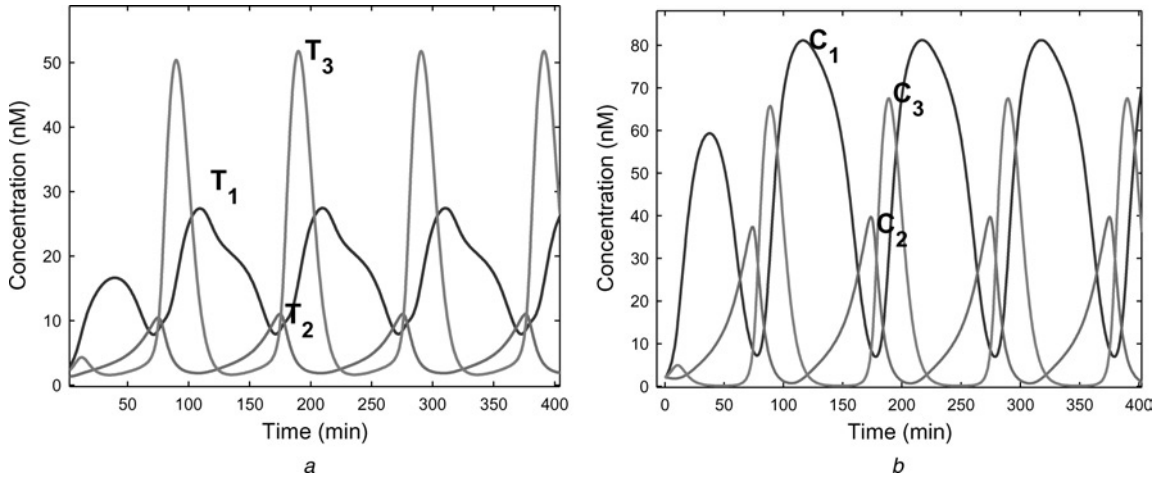

Fig. 12 *Time series of the model for the cell division cycle of budding yeast*

Period of the cycle is approximately 90 min. Eventhough the amplitudes are different, the cell cycle exhibits domino-like transition; that is, there is a step-wise rise and fall of T's *a* and C's *b* in the model

υ_{d_2} is taken as 1.052 for the simulation when the cell is in S-G2-M state; that is, in the unstable state surrounded by stable limit cycle. The other parameters used are from the legend of Fig. 10 and Table 1

4.2 Explanation for the checkpoint point mechanism: silencing of the negative feedback loops and the dominance of positive feedback loops

The bifurcation diagram and the time series are again used to explain the checkpoint mechanism that blocks the progress of the cell cycle under unfavourable conditions in either G1 or S-G2-M phases (Fig. 13). In G1 arrest state both Cln's and Clb's are present at a very low concentration, whereas in the S-G2-M phase arrest, the inhibitors of Clb's are present at a very low concentration. The checkpoint proteins enforces this mechanism by effectively deactivating the cyclins and their inhibitors. The checkpoint mechanism is therefore explained by reducing υ_{10} and υ_{11} which are the rates of cyclin synthesis and υ_{12}, the rate of their inhibitors to a low value in the model. As a consequence, the G1 and S-G2-M arrest state results in the weakening of the ternary homogeneous negative feedback loops and the dominance of the ternary positive feedback loops generated by the interactions among the TFs in the model (Fig. 13 I, II and III). Bifurcation diagram is constructed with υ_{d_2} as the parameter. The G1 checkpoint for the budding yeast cell cycle can be simulated by deactivating either Cln's synthesis or by Clb's synthesis and both these cases are considered. In the first case, the rate of cyclin synthesis Cln's 1–3, namely C_1, is arrested by taking the rate υ_{12} close to zero (0.1). This results in a stable steady state that corresponds to a very low production of Clb2 in the bifurcation diagram (Fig. 13*a*). There are two stable steady states with a low value of Clb2 concentration. In this, one of the stable steady state that coexists with unstable steady state is isolated from other stable steady state and hence called 'Isolas' (inset of Fig. 13*a*). Depending on the initial conditions the cell stays in either one of the steady states, but importantly, the C_2 concentration in both of these steady states are extremely low in comparison with the G1-phase of normal cell cycle (as shown in Fig. 11*a*), suggesting the arrest of cell cycle in G1-phase. The time series of the cyclins and their inhibitors are shown in the right panel of Fig. 13*a* for one particular initial condition. Time series correctly show that in G1 arrest state the inhibitor of cyclins (C_3) is present in large quantity, whereas C_2 is present in a very low concentration. In the second case for G1-checkpoint, the rate of Clb2 (C_2) production υ_{11} is taken close to zero (0.1). There is a steep sigmoidal increase in the concentration of C_2 in the bifurcation diagram, but reaches a saturation concentration (Fig. 13*b*). This steep increase is similar to that Fig. 13*a* and the same saturation concentration level is attained. In the time series, concentration of C_1 is still higher and the inhibitors of the cyclins C_3 is gradually destroyed with the increase of C_1, but C_2 is still at a lower concentration in comparison with the normal cell cycle, suggesting a G1 arrest state. Not only the G1-checkpoint can be simulated by deactivating either Cln's or Clb's concentration individually in the model, but can also be realised by deactivating both Cln's and Clb's rates simultaneously; that is, taking both υ_{11} and υ_{12} close to zero together and this results in the same bifurcation diagram time series as in Fig. 13*a*.

In S-G2-M checkpoint simulation, the cell transits the G1 phase but is arrested in the S-G2-M phase. To simulate this the rate of inhibitors production υ_{10} is taken close to zero (0.1). The cell is committed to division but it is blocked

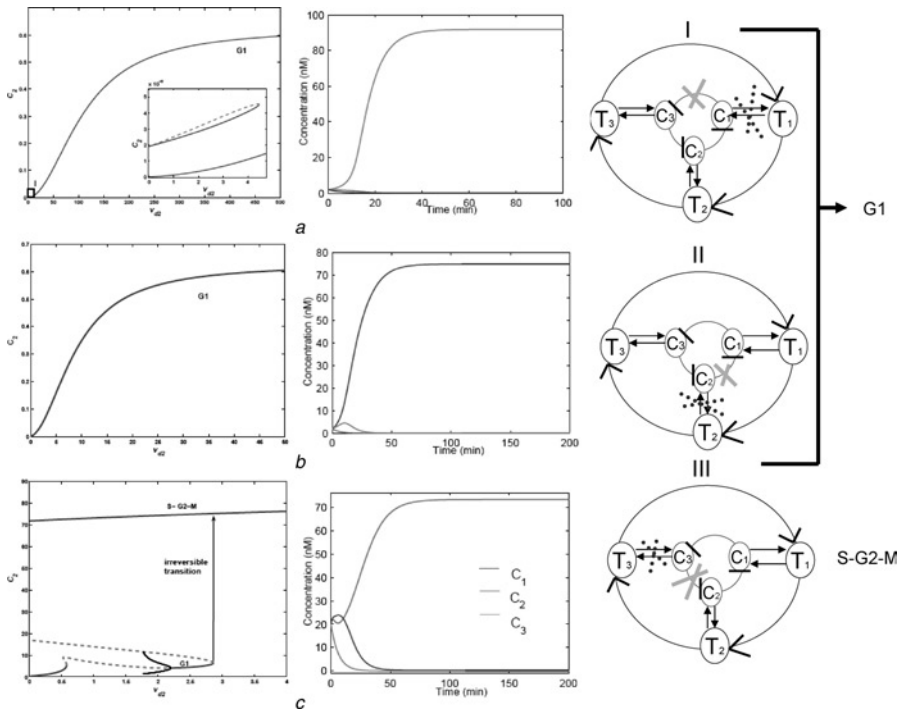

Fig. 13 *Bifurcation diagram and time series for the checkpoints of the budding yeast cell cycle*

Two different checkpoint point controls simulated by varying the rate of cyclins synthesis and their inhibitors υ_{12}, υ_{11} and υ_{10} are shown with υ_{d_2} as the bifurcation parameter. In the extreme right panel is shown the topology of the circuit where the checkpoint mechanism is illustrated through the deactivation of homogeneous ternary negative feedback loops for G1 (I and II) and the S-G2-M phases (III)

The checkpoints can also be simulated by silencing the homogeneous binary positive feedback loops as shown in the dotted cross lines along with negative feedback loops

In the left panel are the bifurcation diagram and the middle panels are the time series. *a* Cell cycle arrested in G1 phase for $\upsilon_{12} = 0.1$

The box 'I' in the top left panel is expanded and shown as inset where there are two steady states for a small value of υ_{d_2} and one of them is isola. In the isola, one stable steady state coexists with unstable steady state that is isolated from another stable steady state

b Cell cycle again arrested in G1 phase for $\upsilon_{11} = 0.1$ and *c*

Cell cycle arrested in S-G2-M phase for $\upsilon_{10} = 0.1$

by the inhibitory signals. As a result there is an irreversible transition from G1 to S-G2-M state (Fig. 13*c*). The concentration of Clb2 is higher because the checkpoint proteins block the inhibitors that involve in the destruction of Clb2. This is shown clearly in the time series. In the S-G2-M phase arrest, the cell may present in any one of the phases depending on the initial conditions. When the cell is present in G1 state, then the cell can still proceed till M-phase, but cannot carry out the next cycle resulting in irreversible transition. The checkpoint mechanism for budding yeast cell cycle is thus well captured in the model where the cell cycle can be blocked in any of the phases by the checkpoint protein by blocking the synthesis of cyclins and their inhibitors. The checkpoint mechanism can also be simulated by silencing the coupling constants k_{c_1}, k_{c_2} and k_{c_3} along with silencing the synthesis of cyclins and their inhibitors (Fig. 13 I, II and III). In the wiring diagram this is equivalent to blocking selectively both the binary positive feedback loop and the ternary negative feedback loop. Therefore in all the checkpoint mechanism, homogeneous ternary positive feedback loops arising out from the sequential regulation of TFs play a very strong role in generating steady-state dynamics and thereby exhibits mostly the stable steady states in the checkpoint mechanism.

5 Discussion, conclusion and future direction of work

In this article, a novel topology of regulatory network abstracted from the experimental data of the budding yeast cell cycle is presented in a modular form. The present study consists of two parts. In the first part, the topology (Fig. 2*c*) is decomposed in to two modules (Fig. 2*a* and *b*) and the dynamics of both the individual and the recomposed modules are thoroughly studied to determine the role played by different feedback loops in the system. The modules consist of the ternary homogeneous positive and negative feedback loops that exhibits bistability and limit cycle oscillations, respectively. The individual modules are modelled with fewer number of variables and parameters. As most of the kinetic constants are not known, biologically plausible parameter values are chosen for this study. The dynamics are found to be robust to parameter variations and exhibit wide regime of bistability and oscillations in the bifurcation diagram (Figs. 3 and 4). When the modules are recomposed by binary positive feedback loops the individual dynamics are mostly retained in apart from other complex dynamics (Fig. 8). The complex dynamics obtained are shown to be the result of varying the strength of the binary positive feedback loop in the regulatory network. The role of this feedback loop is further studied in detail by constructing one and two parameter bifurcation diagrams. Codimension-2 bifurcation diagram revealed TB and Cusp bifurcations (top left and right panel of Fig. 6) and codimension-1 bifurcation diagram revealed multistability and different types of limit cycle oscillations (bottom left and right panels of Fig. 6). Two specific examples are shown to illustrate the importance of the binary positive feedback loops in the model that has relevance in the functioning of the cell division cycle: (i) it induces domino-like oscillations (Figs. 5 and 6) and (ii) it brings in the notion of checkpoint mechanism (Figs. 7*a* and *b*). Most of the dynamics obtained are sensitive to initial conditions and depending on the initial conditions the system may settle down either to the oscillatory or to the stable steady state (Fig. 7*c*). But the stable steady states are not robust as indicated by the addition of small amount of noise that restores the system to its oscillatory state (Fig. 7*d*). Period-doubling route to autonomous chaos has also been observed and chaos coexists with period-1 oscillations (Fig. 14). Period-1 oscillations are found to dominate a very large parameter regime than that of chaotic regime (bifurcation diagram not shown) and therefore the model exhibits predominantly periodic oscillations and not chaotic oscillations. Further, as the type of chaos and its implication in the regulatory network of cell division cycle is not clearly known, it is not pursued further. To summarise the findings in the first part, the role of positive and negative feedback loops, variation in the Hill's coefficent and the feedback mechanism that brings about various types of oscillations are studied in detail by constructing one and two parameter bifurcation diagrams.

In the second part, it is shown that this simple model also can clearly explain the functioning of the cell division cycle of the budding yeast. The two most important characteristic features that the protein network in the cell cycle exhibits are the domino-like oscillations and the checkpoint mechanism [40]. The present model exhibits both these features and this is exploited to explain the functioning of budding yeast cell cycle (Figs. 9 and 10). Checkpoint dynamics in the model arise because of the sequential positive regulation of the TFs, whereas the clock-like behaviour and domino-like oscillations arise because of the sequential negative regulation of the cyclins and their inhibitors. The binary positive feedback loop that links the two ternary homogeneous feedback loops ensures that the dynamics of both the feedback loops are maintained to explain the events that govern the budding yeast cell cycle. However, the present model cannot explain the occurrence of various phenotypes because only the minimal dynamical variables that explains the functioning of the wild-type dynamics are considered.

The complex cell cycle dynamics observed are the same as the one observed by the Tyson and Novak's group in various versions of their model and the checkpoint mechanism is also similar to the one observed by this group [41]. Their models are rigorous and powerful. Yet, the present model differs from their various models in the way the topology of the protein–protein interactions are constructed. Also, the role played by the feedback loops in the normal cell cycle and checkpoint dynamics is entirely different. Though Chen's elaborate models [19, 20], Battogtokh and Tyson's [42] simplified model and Csikasz-Nagy and other's [43] general model have considered TFs, the sequential recruitment of the TFs that provide positive feedback loop are not considered their model. In the present work it is shown clearly that the sequential recruitment of the TFs contributes to bistability and plays a strong role in the checkpoint mechanism. Cyclins and their inhibitors though known to provide bistability is modelled here to exclusively give rise to oscillatory behaviour. The complete cell cycle is shown to be understood when recomposing these two individual modules together by the binary positive feedback loops. This also explains the occurrence of clock-like behaviour and domino-like oscillations in the system. This approach is entirely different from the various models of Tyson's group where, in all their models, only the cyclins and their inhibitors plays a crucial role in generating both bistability and oscillations. However, in the present model, the cyclins and their inhibitors that forms homogeneous negative feedback loop module is abstracted from Tyson and Novak's [18] generic model. Therefore the present model can be thought of as a subset of their simplified model, in which the new information, namely the sequential activation of TFs, is incorporated in the present

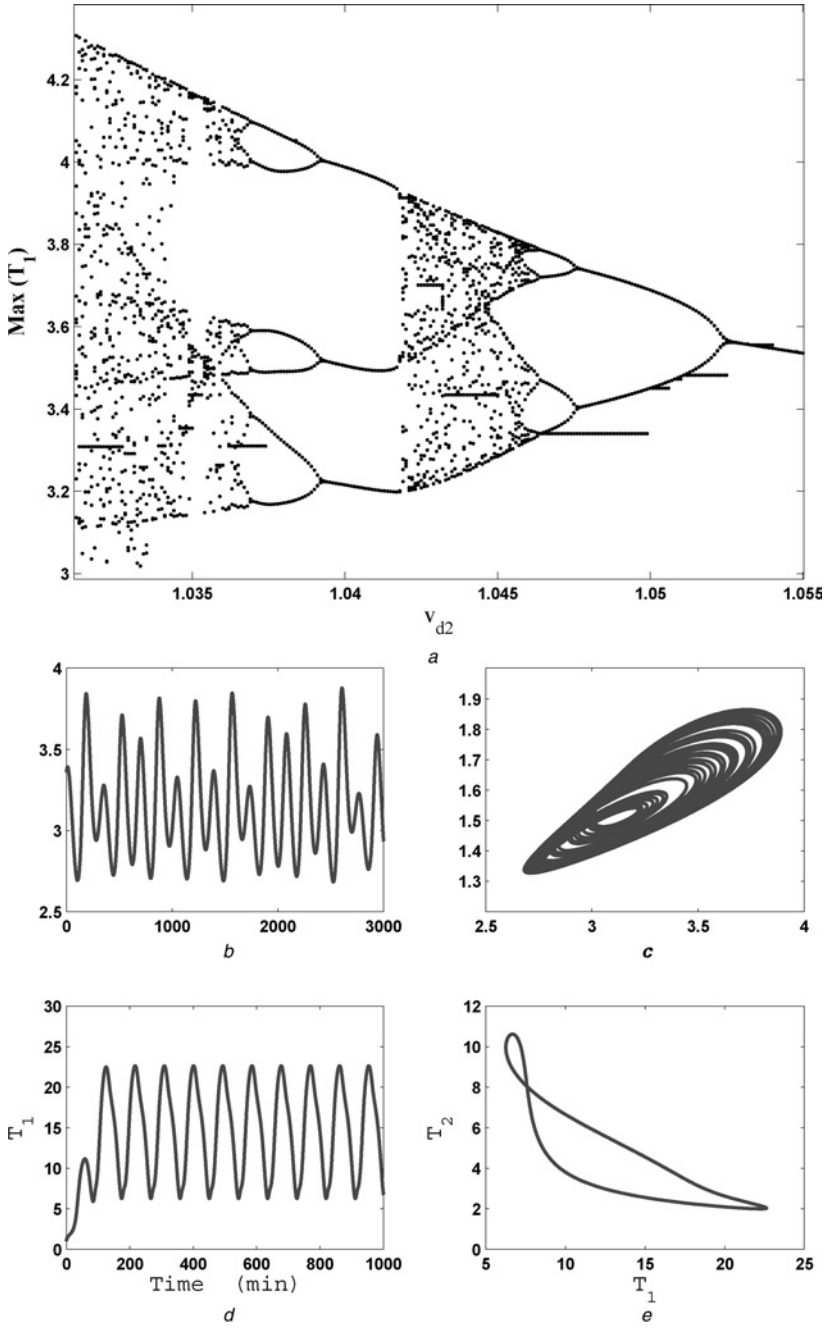

Fig. 14 *Bifurcation diagram, time-series attractors for a constant v_{d_2} and two different initial conditions*

a Inverse period doubling route to chaos is shown for the parameters given in the Table 1. The region of the occurrence of chaos is small and the initial conditions taken for simulating the bifurcation diagram are (3.36, 1.56, 1.36, 8.91, 2.14, 1.02) with a high relative (1×10^{-10}) and absolute tolerances (1×10^{-13}). The other parameters that differs from the parameter set given in Table 1 are $j_2 = 0.5$, $j_3 = 0.21$, $k_{c_1} = k_{c_2} = 0.2$, $k_{c_3} = 0.6$, $v_{d_2} = 3$ and $n = 2$

b and *d* the time series while *c* and *e* the corresponding attractors. Birhythmiticity takes place between chaos and period-1 oscillations

Table 3: Table for one-to-one association with the dynamical variables of the present model with various other species cell division cycle

Dynamical variable	Budding yeast	Fission yeast	Xenopus	Mammalian
T_1	SBF + MBF	cdc10/Res1	XE2F	E2F
T_2	MCM1	–	–	MCM
T_3	ACE2 + SWI5	–	–	–
C_1	Clb2,5	CDC13, Cig2	CycA/B	CycA/B
C_2	Cln1,2,3	Puc1	CycE/CycD	CycE/D
C_3	Sic1,	Rum1, Ste9, Slp1	Xic1, Fzr, Fizzy	$P27^{Kip1}$, hCdh1, $P55^{Cdc}$

study. The present model is also considerably simpler and all the cell cycle dynamics of the wild-type system are captured. We have also compared our model with other cell cycle systems to identify the common dynamical variables so that the model is made generic. This is similar to the one made by Csikasz-Nagy and others [43] and is shown in Table 3. Numerical simulations are not carried out at present, as the present model is specific for budding yeast cell cycle that has no G2 phase. Bifurcation analysis for comparisons with other cell cycles that has clear G2 phase is relegated to the future work.

Also, in future, a more detailed study of the functioning of cell cycle will be taken up by adding few more modules and in particular the modules of MEN and FEAR network [44], to the existing feedback circuits. Efforts will also be directed to distinguish the role of various feedback loops in the functioning of both wild and mutant types of the different yeast cell cycle system.

6 Acknowledgments

We thank Professor Albert Goldbeter for his suggestions and interest in this work. This work is supported by Epigenomics Project, Genopole®. We thank all the referees for their excellent and invaluable comments that has significantly improved the technical content of the manuscript.

7 References

1 Kling, U., and Szekely, G.: 'Simulation of rhythmic nervous activities. I. Function of networks with cyclic inhibitions', *Kybernetik*, 1968, **5**, pp. 89–103
2 Hiernaux, J.: 'Some remarks on the stability of the idiotypic network', *Immunochemistry*, 1977, **14**, pp. 733–739
3 Di Cera, E., Phillipson, P.E., and Wyman, J.: 'Chemical oscillations in closed macromolecular systems', Proc. Natl. Acad. Sci. USA, 1988, 85, pp. 5923–5926
4 Gonze, D., and Goldbeter, A.: 'A model for a network of phosphorylation-dephosphorylation cycles displaying the dynamics of dominoes and clocks', *J. Theor. Biol.*, 2000, **210**, pp. 167–186
5 Elowitz, M.B., and Leibler, S.: 'A synthetic oscillatory network of transcription regulators', *Nature*, 2000, **403**, pp. 335–338
6 Eigen, M., and Schuster, P.: 'The hypercycle: principle of natural self organization' (Springer, Berlin, 1979)
7 Freeman, M.: 'Feedback control of intercellular signalling in development', *Nature*, 2000, **408**, pp. 313–319
8 Tyson, J.J., Chen, K.C., and Novak, B.: 'Sniffers, buzzers, toggles and blinkers: dynamics of regulatory and signalling pathways in the cell', *Curr. Opin. Cell Biol.*, 2003, **15**, pp. 221–231
9 Ferrell, J.E.: 'Self-perpetuating states in signal transduction: positive feedback, double negative feedback and bistability', *Curr. Opin. Cell. Biol.*, 2002, **14**, pp. 140–148
10 Smolen, P., Baxter, D.A., and Byrne, J.H.: 'Modeling circadian oscillations with interlocking positive and negative feedback loops', *J. Neurosci.*, 2001, **21**, pp. 6644–6656
11 Thomas, R., and D'Ari, R.: 'Biological Feedback' (CRC Press, 1990)
12 Thomas, R.: 'Laws for the dynamics of regulatory networks', *Int. J. Dev. Biol.*, 1998, **42**, pp. 479–485
13 Gardner, T.S., Cantor, C.C. and Collins, J.J.: 'Construction of a genetic toggle switch in Escherichia Coli', *Nature*, 2000, **403**, pp. 339–342
14 Becskei, A., Seraphin, B., and Serrano, L.: 'Positive feedback in eukaryotiv gene networks: cell differentiation by the graded to binary response conversion', *EMBO. J*, 2001, **20**, pp. 2528–2531
15 Hasty, J., McMillen, D., and Collins, J.J.: 'Engineered gene circuits', *Nature*, 2002, **420**, pp. 224–230
16 Guet, C.C., Elowitz, M.B., Hsing, W., and Leibler, S.: 'Combinatorial synthesis of genetic networks', *Science*, 2002, **296**, pp. 1466–1470
17 Simon, I., Barnett, J., Hannett, N., Harbison, C.T., Rinaldi, N.J., Volkert, T.L., Wyrick, J.J., Zeitlinger, J., Gifford, D.K., Jaakkola, T.S., and Young, R.A.: 'Serial regulation of transcriptional regulators in the yeast cell cycle', *Cell*, 2001, **106**, pp. 697–708
18 Tyson, J.J., and and Novak, B.: 'Regulation of eukaryotic cell cycle: molecular antagonism, hysteresis and irreversible transitions', *J. Theor. Biol.*, 2001, **210**, pp. 249–263
19 Chen, K.C., Csikasz-Nagy, A., Gyoffry, B., Val, J., Novak, B., and Tyson, J.J.: 'Kinetic analysis of a molecular model of the budding yeast cell cycle', *Mol. Biol. Cell*, 2000, **11**, pp. 369–391
20 Chen, K.C., Calzone, L., Csikasz-Nagy, A., Cross, F.R., Novak, B., and Tyson, J.J.: 'Integrative analysis of a cell cycle control in budding yeast', *Mol. Biol. Cell*, 2004, **15**, pp. 3841–3862
21 Ermentrout, B.: 'XPPAUT 4.0- The differential equation tool, free software'1996, available from http://www.pitt.edu/~phase
22 MATLAB: (The Math Works Inc.), South Natick, Massachusetts, 1989
23 Wolfram, S.: 'The Mathematica 3.0 book' (Wolfram Media/ Cambridge University Press, Cambridge, 1996)
24 Guckenheimer, J., and Holmes, P.: 'Nonlinear oscillations, dynamical systems an bifurcations of vector fields' (Springer, Berlin, 1983)
25 Pomerening, J.R., Kim, S.Y., and Ferrell, J.E.: 'Systems-level dissection of the cell cycle oscillator: bypassing positive feedback produced damped oscillations', *Cell*, 2005, **122**, (4), pp. 565–578
26 Murray, A., and Hunt, T.: 'The cell cycle: An introduction' (OUP, NY, 1993)
27 Mendenhall, M.D., and Hodge, A.E.: 'Regulation of Cdc28 cyclin-dependent protein kinase activity during cell cycle of the yeast *Saccharomyces cerevisiae*', *Microbiol. Mol. Biol. Rev.*, 1998, **62**, pp. 1191–1243
28 Nasmyth, K.: 'Control of the yeast cycle by Cdc28 protein kinase', *Curr. Opin. Cell Biol.*, 1993, **5**, pp. 166–179
29 Nasmyth, K., and Dirick, L.: 'The role of SWI4 and SWI6 in the activity of G1 cyclins in yeast', *Cell*, 1991, **66**, pp. 995–1013
30 Schwob, E., and Nasmyth, K.: 'CLB5 and CLB6, a new pair of B cyclins involved in DNA replication in *Sacchromyces Cerevisiae*', *Genes Devel.*, 1993, **7**, pp. 1160–1175
31 Amon, A., Tyers, M., Futcher, B., and Nasmyth, K.: 'Mechanisms that help the yeast cell cycle clock tick: G2 cyclins transcriptionally activateG2 cyclins G2 cyclins and repress G1 cyclins', *Cell*, 2003, **74**, pp. 993–1007
32 Lee, T.I., Rinaldi, N.J., Robert, F., Odom, D.T., Bar-Joseph, Z., Gerber, G.K., Hannett, N.M., Harbison, C.T., Thompson, C.M., Simon, I., Zeitlinger, J., Jennings, E.G., Murray, H.L., Gordon, D.B., Ren, B., Wyrick, J.J., Tagne, J.B., Volkert, T.L., Fraenkel, E., Gifford, D.K., and Young, R.A.: 'Transcriptional regulatory networks in *Saccharomyces cerevisiae*', *Science*, 2002, **298**, pp. 799–804
33 Schwab, M., Lutum, A.S., and Seufert, W.: 'Yeast Hct1 is a regulator of Clb2 proteolysis', *Cell*, 1997, **90**, pp. 683–693
34 Visintin, R., Prinz, S., and Amon, A.: 'CDC20 and CDH1: a family of substrate specific activators of APC-dependent proteolysis', *Science*, 1997, **278**, pp. 460–463
35 Ogas, J., Andrews, B.J., and Hershkovitz, I.: 'Transcriptional activation of CLN1, CLN2 and a putative new G1 cyclin (HCS26) by SWI4, a positive regulator of G1-specific transcription', *Cell,* 1991, **66**, pp. 1015–1022
36 Cross, F.R., and Tinkenberg, A.H.: 'A potential positive feedback loop controlling CLN1 and CLN2 gene expression at the start of the cell cycle', *Cell*, 1991, **65**, pp. 875–882
37 Maher, M., Cong, F., Kindelberger, D., Nasmyth, K., and Dalton, S.: 'Cell cycle-regulated transcription of CLB2 gene is dependent on Mcm1 and a ternary complex factor', *Mol. cell. Biol.*, 1995, **25**, pp. 3129–3127
38 Knapp, D., Bhoite, L., Stillman, D.J., and Nasmyth, K.: 'The transcription factor Swi5 regulates expression of the cyclin kinaseinhibitor P40Sic1', *Mol. Cell. Biol.*, 1996, **16**, pp. 5701–5707
39 Nasmyth, K.: 'At the heart of the budding yeast cell cycle', *Trends Genet.*, 1996, **12**, pp. 405–412
40 Murray, A.W., and Kirschner, M.W.: 'Dominoes and clocks: the union of two views of cell cycle', *Science*, 1989, **246**, pp. 614–621
41 Tyson, J.J., Csikasz-Nagy, A., and Novak, B.: 'The dynamics of cell cycle regulation', *BioEssays*, 2002, **24**, pp. 1095–1109
42 Battogtokh, D., and Tyson, J.J.: 'Bifurcation analysis of a model of the budding yeast cell-cycle', *Chaos*, 2004, **14**, pp. 653–661
43 Csikasz-Nagy, A., Battogtokh, D., Chen, K.C., Novak, B., and Tyson, J.J.: 'Analysis of a generic model of eukaryotic cell-cycle regulation', *Biophys. J*, 2006, **90**, pp. 4361–4379
44 Bosl, J.W., and Li, R.: 'Mitotic-exit control as an evolved complex system', *Cell*, 2005, **121**, pp. 325–333

8 Appendix

8.1 Linear stability analysis

Linear stability analysis is carried out for (1)–(3) and (4)–(6) separately to determine the nature of bifurcations around the steady state. The steady states are determined by simultaneously taking the rates of (1)–(3) and (4)–(6)

to zero. The equations are linearised around the steady states and the Jacobian is calculated. The nature of bifurcations around the steady state is determined by calculating the eigenvalues of the Jacobian. All these calculations are carried out using MATHEMATICA® [23, 1996]. All the values are taken from the table except $\upsilon_{d_2} = 50$ to determine the steady states T_1s, T_2s, T_3s for (1)–(3). There are three steady states and they are (5.06, 32.57, 6.97), (1.03, 1.28, 0.86) and (1.90, 4.03, 2.89). To determine the stability of these steady states, Jacobian is determined and is given by

$$J = \begin{pmatrix} -k_{d_1} - \lambda & 0 & \dfrac{3k_{m_1}[T_{3s}]^2 \upsilon_{d_1}}{(km_1^3 + T_{3s}^3)^2} \\ \dfrac{3k_{m_2}[T_{1s}]^2 \upsilon_{d_2}}{(km_2^3 + T_{1s}^3)^2} & -k_{d_2} - \lambda & 0 \\ 0 & \dfrac{3k_{m_3}[T_{2s}]^2 \upsilon_{d_3}}{(km_3^3 + T_{2s}^3)^2} & -k_{d_3} - \lambda \end{pmatrix}$$

The characteristic equation is

$$\lambda^3 + (k_{d_1} + k_{d_2} + k_{d_3})\lambda^2 + (k_{d_1}k_{d_2} + k_{d_1}k_{d_3} + k_{d_2}k_{d_3})\lambda + k_{d_1}k_{d_2}k_{d_3} + \frac{27k_{m_1}^3 k_{m_2}^3 k_{m_3}^3 T_{1s}^2 T_{2s}^2 T_{3s}^2 \upsilon_{d_1}\upsilon_{d_2}\upsilon_{d_3}}{(k_{m_2}^3 + T_{1s}^3)^2 (k_{m_3}^3 + T_{2s}^3)^2 (k_{m_1}^3 + T_{3s}^3)^2} = 0$$

The eigen values for the steady state (5.06, 32.57, 6.97) is $-0.92 \pm 0.14i$ and -0.65, for (1.03, 1.28, 0.86) it is $-0.97 \pm 0.23i$ and -0.55 and for (1.90, 4.03, 2.89) it is $-1.49 \pm 1.46i$ and 0.49. The system exhibits bistability where two steady states are stable and one unstable as determined from the eigen-values of the characteristic equation.

The following are the linear stability analysis carried out for (4)–(6). All the values are taken from the table except $\upsilon_{12} = 15$ to determine the steady states C_1s, C_2s, C_3s for the equation (4)–(6). There is only one steady state and is (16.66, 16.66, 16.66) and following are the Jacobian around the steady state and the characteristic equations used to determine the eigen-values of the Jacobian.

$$J = \begin{pmatrix} -k_{d_4} - \lambda & -\dfrac{3C_{2s}^2 k_{120}^2 \upsilon_{12}}{(C_{2s}^3 + k_{120}^3)^2} & 0 \\ 0 & k_{d_5} - \lambda & -\dfrac{3C_{3s}^2 k_{110}^2 \upsilon_{11}}{(C_{3s}^3 + k_{110}^3)^2} \\ -\dfrac{3C_{1s}^2 k_{100}^2 \upsilon_{10}}{(C_{1s}^3 + k_{100}^3)^2} & 0 & -k_{d_6} - \lambda \end{pmatrix}$$

The characteristic equation is

$$\lambda^3 + (k_{d_4} - k_{d_5} - k_{d_6})\lambda^2 + (k_{d_4}k_{d_5} + k_{d_4}k_{d_6} - k_{d_5}k_{d_6})\lambda + k_{d_4}k_{d_5}k_{d_6} - \frac{27k_{100}^2 k_{110}^3 k_{120}^3 c_{1s}^2 c_{2s}^2 c_{3s}^2 \upsilon_{10}\upsilon_{d11}\upsilon_{12}}{(k_{100}^3 + C_{1s}^3)^2 (k_{110}^3 + C_{3s}^3)^2 (k120^3 + C_{2s}^3)^2} = 0$$

The eigen values are -0.55 and $0.04 \pm 0.04i$, where the real part of the complex root is unstable and points to unstable focus. This suggests that the HB is supercritical in nature, where the unstable focus become stable limit cycle. The supercritical HB is shown in Fig. 3.

For the same parameter set with Hills' coefficient $n = 2$, the steady states C_1s, C_2s, C_3s for (4)–(6) is (19.51, 19.51, 19.51). The eigen values are -0.41 and $-0.03 \pm 0.03i$, where the real part of the complex root is negative and points to stable focus. Thus, the limit cycle oscillations are not possible for $n = 2$.

Linear stability analysis cannot be performed for (7)–(10) because of the high dimension of the system. So bifurcation analysis is directly carried out for these equations using the software XPPAUT.